arXiv:1304.6320v1 [cond-mat.mes-hall] 23 Apr 2013

Graphene Based Plasmonic Tunable Low Pass Filters in the THz Band

D. Correas Serrano,[1,*] **J. S. Gomez Diaz,**[2] **J. Perruisseau-Carrier** [2]
and A. Alvarez Melcon[1]

[1] *Universidad Politecnica de Cartagena, Departamento TIC, 30202 Cartagena (Murcia), Spain*

[2] *Adaptive MicroNanoWave Systems, LEMA/Nanolab, École Polytechnique Fédérale de Lausanne, 1015 Lausanne, Switzerland*
[*] *diego.correas.serrano@gmail.com*

Abstract: We propose the concept, synthesis, analysis and design of graphene-based plasmonic tunable low-pass filters operating in the THz band. The proposed structure is composed of a chemically-doped graphene strip deposit on a dielectric and a set of polysilicon DC gating pads located beneath it. This structure implements a stepped impedance low-pass filter for the propagating surface plasmons by adequately controlling the guiding properties of each strip section through graphene's field effect. A synthesis procedure is presented to design filters with desired specifications in terms of cut-off frequency and in-band and rejection characteristics. The electromagnetic modeling of the structure is efficiently performed by combining an electrostatic scaling law to compute the guiding features of each strip section with a transmission line and transfer-matrix framework, which is also validated via full wave simulations. Excellent performance is obtained for this frequency range in terms of roll-off, insertion losses (≈ 3 dB assuming a graphene relaxation time of $\tau = 1$ ps) and reconfiguration capabilities (around 50%). These results, together with the high miniaturization associated with plasmonic propagation, are very promising for the future use and integration of the proposed filters with other graphene and silicon-based elements in innovative THz communication systems.

References and links

1. Q. Bao and K. P. Loh, "Graphene photonics, plasmonics, and broadband optoelectronic devices," ACS Nano **6**, 3677–3694 (2012).
2. J. Perruisseau-Carrier, "Graphene for antenna applications: Opportunities and challenges from microwaves to thz," in "Antennas and Propagation Conference (LAPC)," (Loughborough (UK), 2012), pp. 1–4.
3. P. Y. Chen and A. Alu, "All-graphene terahertz analog nanodevices and nanocircuits," in "European Conference on Antennas and Propagation," (Gothenburg, Sweden, 2013).
4. J. F. Federici, B. Schulkin, F. Huang, D. Gary, R. Barat, F. Oliveira, and D. Zimdars, "Thz imaging and sensing for security applications: explosives, weapons and drugs," Semiconductor Science and Technology **20**, S266 (2005).
5. A. Rogalski, "Infrared detectors: status and trends," Progress in quantum electronics **27**, 59–210 (2003).
6. V. Lubecke, K. Mizuno, and G. Rebeiz, "Micromachining for terahertz applications," Microwave Theory and Techniques, IEEE Transactions on **46**, 181–1831 (1998).
7. M. Jablan, H. Buljan, and M. Soljacic, "Plasmonics in graphene at infrared frequencies," Physical review B **80**, 245435 (2009).
8. A. Y. Nikitin, F. Guinea, F. J. García-Vidal, and L. Martín-Moreno, "Edge and waveguide terahertz surface plasmon modes in graphene microribbons," Phys. Rev. B **84**, 161407 (2011).
9. J. Christensen, A. Manjavacas, S. Thongrattanasiri, F. H. L. Koppens, and F. J. G. de Abajo, "Graphene plasmon waveguiding and hybridization in individual and paired nanoribbons," ACS Nano **6**, 431–440 (2012).

10. J. S. Gómez-Díaz and J. Perruisseau-Carrier, “Propagation of hybrid transverse magnetic-transverse electric plasmons on magnetically-biased graphene sheets,” Journal of Applied Physics **112**, 124906 (2012).
11. M. Tamagnone, J. S. Gómez-Díaz, J. R. Mosig, and J. Perruisseau-Carrier, “Reconfigurable thz plasmonic antenna concept using a graphene stack,” Applied Physics Letters **101**, 214102 (2012).
12. R. Filter, M. Farhat, M. Steglich, R. Alaee, C. Rockstuhl, and F. Lederer, “Tunable graphene antennas for selective enhancement of thz-emission,” Optics Express **21**, 3737–3745 (2013).
13. E. Carrasco and J. Perruisseau-Carrier, “Tunable graphene reflective cells for thz reflectarrays and generalized law of reflection,” Applied Physics Letters **102**, 104103 (2013).
14. F. Rana, “Graphene terahertz plasmon oscillators,” IEEE Trans. Nanotech. **7**, 91–99 (2008).
15. J. S. Gómez-Díaz and J. Perruisseau-Carrier, “Graphene-based plasmonic switches at near infrared frequencies,” Preprint arXiv:1302.0770 (2-013).
16. B. Sensale-Rodriguez, R. Yan, M. M. Kelly, T. Fang, K. Tahy, W. S. Hwang, D. Jena, L. Liu, and H. G. Xing, “Broadband graphene terahertz modulators enabled by intraband transitions,” Nature Communications **3**, 780 (2012).
17. A. Fallahi and J. Perruisseau-Carrier, “Design of tunable biperiodic graphene metasurfaces,” Physical Review B **86**, 195408 (2012).
18. P. Y. Chen, C. Argyropoulos, and A. Alu, “Terahertz antenna phase shifters using integrally-gated graphene transmission-lines,” IEEE Transactions on Antennas and Propagation (2013).
19. R. Arsat, M. Breedon, M. Shafiei, P. G. Spizziri, S. Gilje, R. B. Kaner, K. Kalantar-zadeh, and W. Wlodarski, “Graphene-like nano-sheets for surface acoustic wave gas sensor applications,” Chemical Physics Letters **467**, 344–347 (2009).
20. X. Kang, J. Wang, H. Wu, J. Lui, I. A. Aksay, and Y. Lin, “A graphene-based electrochemical sensor for sensitive detection of paracetamol,” Talanta **81**, 754–759 (2010).
21. F. Schuster, D. Coquillat, H. Videlier, M. Sakowicz, and F. T. et al, “Broadband terahertz imaging with highly sensitive silicon cmos detectors,” Optics Express **19**, 7827–7832 (2011).
22. S. Boppel, A. Lisauskas, V. Krozer, and H. Roskos, “Performance and performance variations of sub-1 thz detectors fabricated with 0.15 μm cmos foundry process,” Electronics Letters **47**, 661–662 (2011).
23. A. Hosseini, H. Nejati, and Y. Massoud, “Design of a maximally flat optical low pass filter using plasmonic nanostrip waveguides,” Optics Express **15** (2007).
24. X.-S. Lin and X.-G. Huang, “Tooth-shaped plasmonic waveguide filters with nanometeric sizes,” Optic Letters **33** (2008).
25. J. H. Zhu, Q. J. Wang, P. Shum, and X. G. Huang, “A nanoplasmonic high-pass wavelength filter based on a metal-insulator-metal circuitous waveguide,” IEEE Transactions on Nanotechnology **10** (2011).
26. V. P. Gusynin, S. G. Sharapov, and J. B. Carbotte, “On the universal ac optical background in graphene,” New J. Physics **11**, 095013 (2009).
27. Z. Fang, S. Thongrattanasiri, A. Schlather, Z. Liu, and L. M. et al, “Gated tunability and hybridization of localized plasmons in nanostructured graphene,” ACS Nano **7**, 2388–2395 (2013).
28. J. S. Gómez-Díaz and J. Perruisseau-Carrier, “A transmission line model for plasmon propagation on a graphene strip,” in “International Microwave Symposium,” (2013).
29. R. J. Cameron, R. Mansour, and C. M. Kudsia, *Microwave Filters for Communication Systems: Fundamentals, Design and Applications* (Wiley-Blackwell, 2007).
30. D. Pozar, *Microwave Engineering* (John Wiley and Sons, 2005), 3rd ed.
31. L. Fan, M. Y. Li, and K. Chang, “Circular waveguide to microstrip transitions,” Electronics Letters **31**, 294–295 (1995).

---

1. Introduction

The unique electrical and optical properties of graphene and its ability to support ultra-confined low-loss plasmons are paving the road to the development of all-integrated graphene plasmonic devices at THz frequencies [1, 2, 3]. These devices may find application in different areas such as chemical and biological remote sensing, high resolution imaging and tomography, time-domain spectroscopy, atmospheric monitoring, and broadband picocellular or intrasatellite communication networks [4, 5, 6]. The desired integrated plasmonic structure must perform multiple complex functions, including signal detection, processing, and transmission. Currently, graphene-based plasmonic components ranging from waveguides [7, 8, 9, 10], antennas [11, 12], reflectoarrays [13], amplifiers [14], switches [15], modulators [16], reconfigurable frequency-selective surfaces [17], or phase-shifters [18] to sensors [19, 20] have already been proposed and investigated.

Terahertz systems also require filtering elements to select target frequency bands and re-

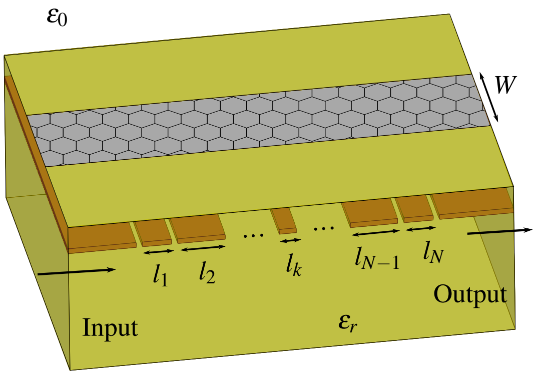

Fig. 1: Proposed graphene-based THz low pass filter of N^{th} degree. The structure consists of a monolayer graphene strip and N gating pads located beneath it.

ject thermal radiation that may otherwise saturate sensitive detectors [21, 22]. Although several plasmonic guided filters have been developed at THz using noble metals and composite structures [23, 24, 25], graphene may lead to the development of novel filters with enhanced performance in terms of reconfiguration capabilities, miniaturization, insertion losses, and integration with other silicon-based elements. However, the use of graphene for the design of such components has not been investigated yet.

In this context, we propose the concept, analysis, and design of graphene-based plasmonic tunable low-pass filters. The structure is composed by a chemically-doped graphene strip and several independent polysilicon DC gating pads located beneath it. The strip supports the propagation of extremely-confined transverse-magnetic (TM) plasmons [8, 9] whose guiding characteristics can be dynamically modified along the line by applying different DC bias voltages to the gating pads. In case that all pads are equally biased, the structure behaves as a simple plasmonic transmission line (TL) propagating the input waves towards the output port. When a different DC bias is applied to a gating pad, the guiding properties of the strip area located above are modified thanks to graphene's field effect. We apply this geometry to implement stepped impedance low pass filters, which are composed of a cascade of transmission lines alternating sections of high and low characteristic impedance. Importantly, the cutoff frequency of the filters can be dynamically tuned by simultaneously modifying the DC bias applied to the gates. A synthesis procedure is then presented to design filters with the desired cutoff frequency and in-band and rejection characteristics, directly providing the physical length of the gating pads and the required biasing voltages. The electromagnetic modeling of the structure is performed combining a transmission line model with a transfer-matrix approach. To this purpose, the recently introduced graphene electrostatic scaling law [9] is applied to efficiently compute the propagation constant of the modes supported by the strip as a function of its width, surrounding media, and applied electrostatic DC bias. The proposed approach allows the accurate analysis of the desired filters in just seconds, avoiding large simulation times of general purpose full-wave software.

In order to illustrate these concepts, several low-pass filters are designed and analyzed, evaluating their performance and reconfiguration capabilities in the THz band. These initial results are very promising for the integration of graphene-based filters in future THz plasmonic devices and communication systems.

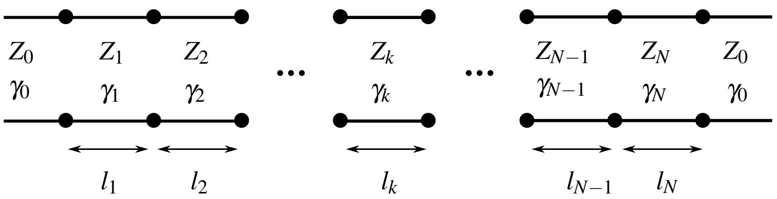

Fig. 2: Equivalent transmission line model of the graphene-based filter shown in Fig 1.

2. Proposed structure

The proposed structure, depicted in Fig. 1, comprises a chemically doped graphene ribbon deposited on a dielectric substrate, and a number of polysilicon gating pads beneath the strip. Graphene can be characterized by a complex-valued surface conductivity σ, which can be modeled using the well-known Kubo formalism [26], and mainly depends on graphene chemical potential μ_c, relaxation time τ and temperature. One of the most interesting features of graphene is that its chemical potential can be tuned over a wide range (typically from -1 eV to 1 eV) by applying a transverse electric field via a DC biased structure, such as the one proposed here. An approximate closed-form expression to relate μ_c and the applied DC voltage (V_{DC}) is given by

$$\mu_c \approx \sqrt{\frac{\pi C_{ox} V_{DC}}{q}}, \tag{1}$$

where $C_{ox} = \varepsilon_r \varepsilon_0 / t$ is the gate capacitance, and ε_r and t are the permittivity and thickness of the gate dielectric. Promising measurements have recently been reported in [27], where a variation in the chemical potential from 0.2 to 0.6 eV was obtained by applying a bias voltage from 0.2 to 1.73 V.

In addition, graphene monolayers support the propagation of surface plasmons polaritons (SPP) at THz frequencies with moderate losses and extreme confinement. Several authors have studied the characteristics of the SPPs propagating along graphene ribbons [8, 9], and transmission line models have been successfully utilized to describe this type of structure [14, 28]. Using this approach, the structure of Fig. 1 can be modeled as a cascade of transmission lines, as shown in Fig. 2. The complex-valued characteristic impedance and propagation constant of the transmission lines depend on graphene's chemical potential and will be largely modified by the DC voltage applied to the gating pads, allowing the synthesis of the proposed filters.

3. Synthesis and Modeling of Graphene-based Filters

3.1. Synthesis Procedure

The goal of this section is to design a lowpass filter using the structure of Fig. 1, with the desired cutoff frequency, rejection characteristics and inband performance. This structure implements a so-called stepped impedance lowpass filter [29], whose equivalent network is presented in Fig. 2. As seen, it is composed of the connection of N transmission line sections with lengths l_k, propagation constants γ_k and characteristic impedances Z_k.

The design procedure starts with the calculation of transfer and reflection polynomials to satisfy the desired specifications in terms of in-band and rejection characteristics (order of the filter, rejection level, return losses)

$$S_{21}(\omega) = \frac{1}{\varepsilon E(\omega)}, \qquad S_{11} = \frac{F(\omega)}{E(\omega)} \tag{2}$$

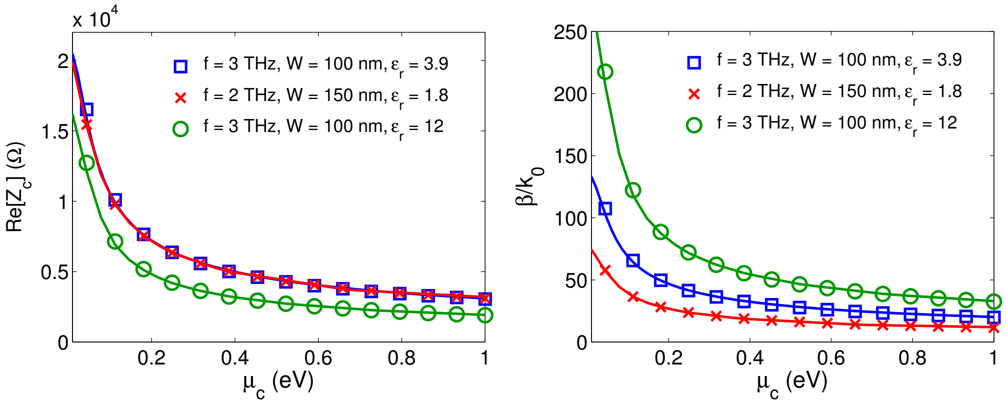

(a)

(b)

Fig. 3: Characteristic impedance (a) and normalized phase constant (b) of the first waveguide-like surface plasmon propagating along different graphene strip configurations versus the chemical potential μ_c. Solid lines have been obtained using the electrostatic approach described in Section III and markers indicate values computed with HFSS. Graphene parameters are $\tau = 1$ ps and $T = 300$ K.

The calculation of the $P(s)$ and $E(s)$ polynomials is done analytically for most useful transfer functions, including Butterworth and generalized Chebyshev responses. Some useful techniques are reported in [29]. The next step in the design procedure is the election of the electrical length θ_c of the individual line sections. This parameter directly determines the periodicity of the frequency response when the ideal polynomials are implemented with transmission lines. Smaller values of θ_c result in a wider spurious-free range, while requiring more abrupt changes in the line impedances. Having decided the value of θ_c, a recursive technique [29] is applied to extract the normalized values of characteristic impedances ($\bar{Z}_k$). Then, the de-normalization of the calculated characteristic impedances to the real port impedances (Z_0) used in the filter implementation is done as $Z_k = \bar{Z}_k Z_0$.

The final and crucial design step consists in finding the design parameters of the physical structure in Fig. 1, to implement the prototype circuit at the desired cut-off frequency. To this purpose, the required de-normalized impedance values (Z_k) obtained during the above procedure are synthesized using the SPP properties of graphene strips. This can be most efficiently accomplished by adjusting appropriate chemical potentials (μ_c) through electrostatic gating. As an illustrative example of this electrical control, we show in Fig. 3 the real part of the characteristic impedance and normalized phase constant of the first waveguide-like mode propagating along a graphene strip, computed versus the chemical potential for graphene waveguides of different characteristics. In our work we have decided to maintain fixed the width of all the strips, and to adjust the impedances of all sections (Z_k) by acting only on the chemical potential by applying an electrostatic gating. It can be observed in the figure that, for several strip widths and frequencies, the impedances that can be obtained vary from around 20 kΩ to several hundreds of ohms for practical chemical potentials in the range $0-1$ eV. Note that the calculation of the chemical potentials for all sections, following this procedure, also fixes the values of their propagation constants (β_k). This information, and the election of (θ_c) done during the synthesis phase, allows the calculation of the physical lengths of all graphene strip sections in Fig. 1 with the straightforward relation

$$l_k = \frac{\theta_c}{\beta(\mu_c)} \tag{3}$$

Note that this synthesis procedure is strictly valid when lossless transmission lines are considered. The presence of losses in the real structure leads to small deviations between the actual filter response and the expected synthesized function [29], with some extra round-off inside the filter passband.

3.2. Electromagnetic Modeling

The electromagnetic modeling of the structure shown in Fig. 1 is based on the analysis of its equivalent network (see Fig. 2) using a transmission line formalism combined with an ABCD transfer-matrix approach [30]. The main difficulty of this approach is to accurately compute the complex propagation constant and characteristic impedance of the surface plasmons propagating along each section of the strip. The properties and dispersion relation of these plasmons have been studied by several authors [8, 9]. Unfortunately, the desired dispersion relation does not admit an analytical solution and one has to resort to full-wave numerical techniques. Consequently, the use of the transmission line approach requires the numerical analysis of several graphene strips, which is a tedious and time-consuming task and does not incorporate any advantage over performing the full-wave analysis of the whole structure.

In this context, [9] studied the electrostatic nature of surface plasmon propagating along graphene strips and proposed a simple scaling law able to obtain general dispersion relations. This electrostatic approach, which assumes that the strip width is much smaller than the wavelength, establishes that plasmon properties are solely determined by the strip width (W), surrounding media (ε_r), and graphene conductivity (σ). Then, once the propagating features of a given plasmonic mode have been obtained, they can be scaled to any arbitrary situation (in terms of W, ε_r and σ) by using the scaling parameter

$$\eta(\beta, W) = \chi \frac{\mathrm{Im}[\sigma(f_\beta)]}{f_\beta W}, \tag{4}$$

where $\chi = 2/(\varepsilon_r + 1)$ is a constant that models the dielectric media and f_β is the frequency where the surface plasmon propagates with a phase constant β. Note that, due to the electrostatic approach employed to derive Eq. 4 (see [9]), the scaling parameter η is independent of the operation frequency.

This scaling law is applied to efficiently compute the SPP propagating features along any graphene strip. The process is as follows. First, the scaling parameter η related to the desired surface mode is obtained. To this purpose, a single run of full-wave simulations is required to obtain the dispersion relation of the mode, thus allowing to compute η using Eq. 4. Fig. 4 confirms that η only depends on the product βW [9] and that surface plasmons propagating on different strips leads to the same scaling parameter. Second, the phase constants of surface plasmons propagating along strips of arbitrary characteristics are computed using η. To this purpose, the scaling parameter is computed at the desired operation frequency f_β and strip width W using Eq. 4 and then the corresponding value of βW is interpolated using the information of Fig. 4. Since the strip width W is known, the phase constant of the surface plasmon is easily obtained. Finally, the attenuation constant is found as $\alpha = 1/(2L_p)$, where L_p is the $1/e$ decay distance of the power. The propagation distance of plasmons is mainly controlled by the electron relaxation time of graphene τ, and it can be approximately obtained by $v_g\tau$, where v_g is the plasmon's group velocity ($v_g = \mathrm{d}\omega_p/\mathrm{d}\beta$) [9]. Therefore, the attenuation constant may be

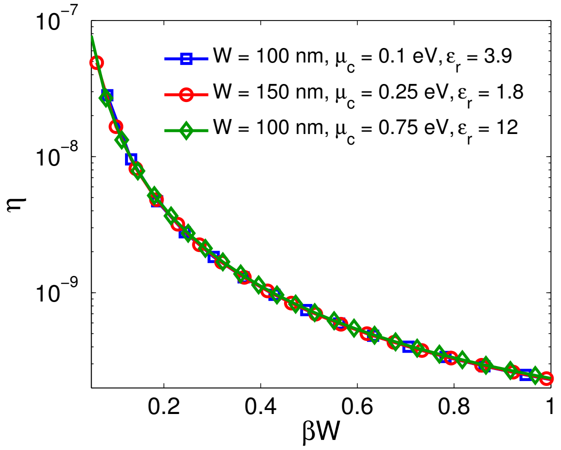

Fig. 4: Scaling parameter η versus the product of the phase constant and the strip width (βW) for different graphene strip configurations. Graphene parameters are $\tau = 1$ ps and $T = 300°$ K.

expressed as

$$\alpha = \frac{1}{2v_g\tau} \tag{5}$$

Once the complex propagation constant $\gamma = \alpha + j\beta$ of the propagating TM plasmon is known, its characteristic impedance is obtained as [30]

$$Z_C = \frac{\gamma}{j\omega\varepsilon_0\varepsilon_{eff}}, \tag{6}$$

where $\varepsilon_{eff} = (1+\varepsilon_r)/2$. The accuracy of this approach is validated in Fig. 3, where the characteristic impedance and phase constant of plasmons propagating along different strip configurations are computed using both the proposed technique and the finite element method (FEM) software HFSS. There, the graphene strip is modeled as an infinitesimally thin layer where surface impedance boundary conditions are imposed ($Z_{surf} = 1/\sigma$.)

The combination of the graphene strip scaling law with a transmission line and transfer-matrix approach permits an extremely fast electromagnetic analysis of the proposed filtering structure (see Fig. 1), allowing an efficient implementation of the synthesis technique described in the previous section. For validation purposes, the electromagnetic response of the complete proposed structure is also obtained using the full-wave software package HFSS.

4. Results and discussion

In this section we design and analyze two low-pass filters which are implemented using the structure shown Fig. 1. For the sake of generality, the filters have been designed to have different order and cutoff frequencies, considering various strip widths and dielectrics. The performance of the filters is presented in terms of their scattering parameters, referred to the characteristic impedance of the graphene sections at the input and output ports. A comparison between the transmission line model combined with the scaling law and full-wave results using HFSS is shown for both cases, validating the accuracy of the proposed electromagnetic modeling. In addition, the reconfiguration capabilities of the filters are investigated in detail. In our study, we consider graphene with a relaxation time τ of 1 ps and a temperature of $T = 300°$ K.

Table 1: Design parameters of the first example: a 7th degree filter.

Section	$\bar{Z}$	l (nm)	$\mu_{c,nominal}$ (eV)	$\mu_{c,tuned1}$ (eV)	$\mu_{c,tuned2}$ (eV)
Ports	1	500	0.17	0.27	0.41
1,7	1.37	382	0.1	0.15	0.23
2,6	0.57	929	0.51	0.74	1
3,5	2.26	232	0.026	0.06	0.1
4	0.45	1172	0.79	1	1

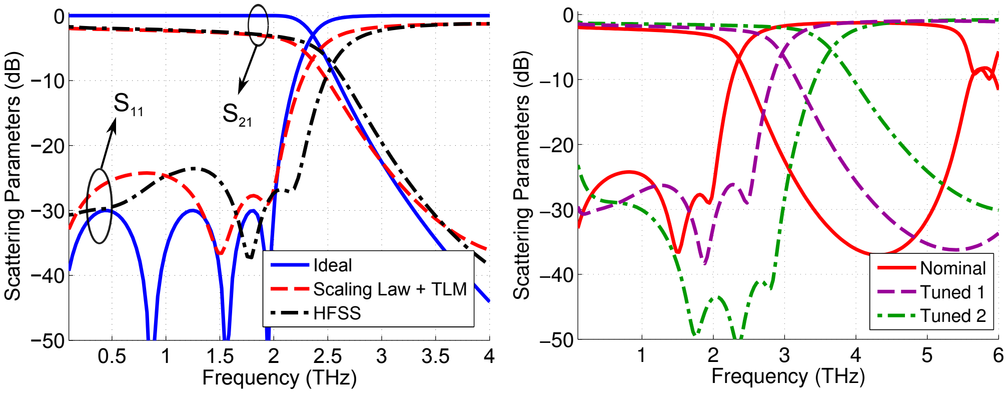

(a)

(b)

Fig. 5: Scattering parameters of a 7^{th} degree filter implemented using the structure depicted in Fig. 1. The design parameters are shown in Table 1, the strip width is 150 nm and ion gel of $\varepsilon_r = 1.8$ is employed as a dielectric. (a) Nominal filter designed to have a cutoff frequency of 2.3 THz. Results are obtained using the ideal synthesis procedure, the transmission line approach combined with the scaling law, and the commercial software HFSS. (b) Reconfiguration possibilities of the filter obtained by adequately controlling the DC bias of the different gating pads.

In the first example, we consider a graphene strip of 150 nm deposited on an ion gel dielectric of permittivity 1.8 [27]. Using this host waveguide, we have designed a 7^{th} degree filter with a cutoff frequency of 2.3 THz. The Chebyshev polynomials were computed using standard techniques [29] for a maximum theoretical return loss of 30 dB, and the electrical length θ_c at the cutoff frequency was set to 37°. These values were chosen to yield practical values of chemical potential through the synthesis procedure explained in the previous section. The final design parameters of the filter are shown in Table 1. Note that filters of this degree with better roll-off characteristics could be synthesized, but this would further increase the required range of chemical potential values achievable in the structure.

Fig. 5a shows the frequency response of the filter, computed using the proposed transmission line approach and the full-wave commercial software HFSS. A good degree of agreement is observed, with very similar attenuation profile and average level of return loss in the passband. Moreover, the structure presents a low insertion loss level, around 3 dB, which is a remarkable value at this frequency range. Insertion losses increase for lower values of graphene's relaxation

Table 2: Design parameters of the second example: a 9th degree filter.

Section	$\bar{Z}$	l (nm)	$\mu_{c,nominal}$ (eV)	$\mu_{c,tuned1}$ (eV)	$\mu_{c,tuned2}$ (eV)
Ports	1	200	0.17	0.35	0.46
1,9	1.36	156	0.1	0.21	0.274
2,8	0.58	367	0.43	0.93	1
3,7	2.24	94	0.035	0.01	0.12
4,6	0.44	483	0.69	1	1
5	2.48	85	0.023	0.078	0.1

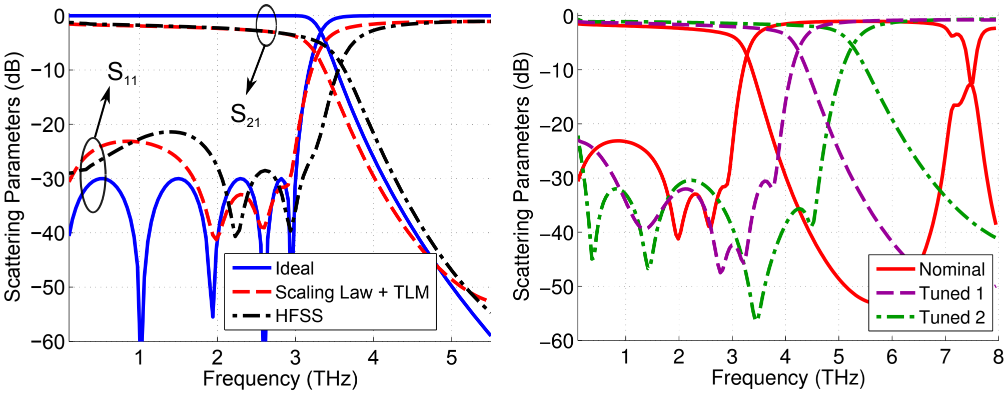

(a)

(b)

Fig. 6: Scattering parameters of a 9^{th} degree filter implemented using the structure depicted in Fig. 1. The design parameters are shown in Table 2, the strip width is 100 nm and quartz of $\varepsilon_r = 3.9$ is employed as a dielectric. (a) Nominal filter designed to have a cutoff frequency of 3.3 THz. Results are obtained using the ideal synthesis procedure, the transmission line approach combined with the scaling law, and the commercial software HFSS. (b) Reconfiguration possibilities of the filter obtained by adequately controlling the DC bias of the different gating pads.

time, but due to the short length of the structure in terms of the plasmon wavelength, they remain at acceptable levels (≈ 5 dB for a relaxation time of $\tau = 0.5$ ps). The slight difference in the cutoff frequency between both approaches is due to the mono-modal nature of the transmission line approach, which neglects the possible excitation of higher order modes at the connection between two adjacent sections. This phenomenon modifies the phase condition of the circuit, which is now fulfilled at a slightly different cutoff frequency. Interestingly, this effect appears to be uniform along the structure, allowing to adjust the filter's cutoff frequency by a small overall scaling of the section lengths. Fig. 5b illustrates the reconfiguration possibilities of the designed filter. By adequately controlling the DC voltage applied to the gating pads, following the synthesis procedure described in Section III, the overall electrical length of the device can be modified thus leading to an electric control of the filter's cutoff frequency.

For the sake of clarity, only two different possible reconfiguration states are shown in the figure (their corresponding design parameters are shown in Table 1). However, a continuous range of cutoff frequencies can be easily synthesized. Importantly, the proposed filter allows a dynamic control of the cutoff frequency over 50%. This value is mainly limited by two factors. First, the fixed physical length of the gating pads imposes a limit to the maximum frequency shift attainable while maintaining an acceptable variation to the attenuation profile and return loss. And second, the values of the chemical potential employed are limited, by technological reasons [31], to the range of $0-1$ eV.

The second example is based on a waveguide of different characteristics, composed of a strip width of 100 nm deposited on a quartz substrate of $\varepsilon_r = 3.9$. The filter's degree has been increased to $N = 9$, and the cutoff frequency is set to 3.3 THz, with $\theta_c = 39°$. The complete design parameters of the filter are shown in Table 2 and the frequency response is plotted in Fig. 6a. Very similar conclusions compared to the previous design can be drawn from the filter response. Importantly, the difference in the cutoff frequency between the two electromagnetic analysis is also of similar relative magnitude to that of the previous example. Finally, the tunable features of this filter are shown in Fig. 6b, where around 50% of cutoff frequency dynamic control is obtained.

5. Conclusion

We have proposed and analyzed graphene-based plasmonic low-pass filters in the THz band. An efficient synthesis method has been presented, based on classical microwave filter theory adapted to graphene SPPs through a recently introduced electrostatic scaling law. Several results, verified with full-wave simulations, showcase the filtering capabilities of the proposed structure and its enhanced performance compared to the alternatives in this frequency range, in terms of roll-off, miniaturization and real-time reconfigurability. In particular, through adequate use of electrostatic gating, the cut-off frequency of the device can be continuously tuned over a wide frequency range, resulting in a degree of tunability not achievable with any other existing technology in the THz band. We envision that the proposed reconfigurable filtering structures may be useful in future all-integrated graphene plasmonic THz devices, sensors and communication systems.

Acknowledgment

This work was supported by the Swiss National Science Foundation (SNSF) under grant 133583 and by the EU FP7 Marie-Curie IEF grant Marconi, with ref. 300966, Spanish Ministry of Education under grant TEC2010-21520-C04-04, and European Feder Fundings. The authors wish to thank Mr. A. Manjavacas (CSIC, Spain) for fruitful discussions.